

Available online at [www.sciencedirect.com](http://www.sciencedirect.com)

ScienceDirect

[www.elsevier.com/locate/jmbbm](http://www.elsevier.com/locate/jmbbm)

## Research Paper

# Mechanical properties of gray and white matter brain tissue by indentation



Silvia Budday<sup>a</sup>, Richard Nay<sup>b</sup>, Rijk de Rooij<sup>c</sup>, Paul Steinmann<sup>a</sup>,  
Thomas Wyrobek<sup>b</sup>, Timothy C. Ovaert<sup>d</sup>, Ellen Kuhl<sup>c,e,\*</sup>

<sup>a</sup>Chair of Applied Mechanics, University of Erlangen-Nuremberg, 91058 Erlangen, Germany

<sup>b</sup>Hysitron, Inc., Eden Prairie, MN 55344, USA

<sup>c</sup>Department of Mechanical Engineering, Stanford University, Stanford, CA 94305, USA

<sup>d</sup>Department of Aerospace and Mechanical Engineering, The University of Notre Dame, Notre Dame, IN 46556, USA

<sup>e</sup>Department of Bioengineering, Stanford University, Stanford, CA 94305, USA

## ARTICLE INFO

## Article history:

Received 23 November 2014

Received in revised form

20 February 2015

Accepted 23 February 2015

Available online 2 March 2015

## Keywords:

Brain

Gray matter

White matter

Indentation

Viscoelasticity

## ABSTRACT

The mammalian brain is composed of an outer layer of gray matter, consisting of cell bodies, dendrites, and unmyelinated axons, and an inner core of white matter, consisting primarily of myelinated axons. Recent evidence suggests that microstructural differences between gray and white matter play an important role during neurodevelopment. While brain tissue as a whole is rheologically well characterized, the individual features of gray and white matter remain poorly understood. Here we quantify the mechanical properties of gray and white matter using a robust, reliable, and repeatable method, flat-punch indentation. To systematically characterize gray and white matter moduli for varying indenter diameters, loading rates, holding times, post-mortem times, and locations we performed a series of  $n = 192$  indentation tests. We found that indenting thick, intact coronal slices eliminates the common challenges associated with small specimens: it naturally minimizes boundary effects, dehydration, swelling, and structural degradation. When kept intact and hydrated, brain slices maintained their mechanical characteristics with standard deviations as low as 5% throughout the entire testing period of five days post mortem. White matter, with an average modulus of  $1.895 \text{ kPa} \pm 0.592 \text{ kPa}$ , was on average 39% stiffer than gray matter,  $p < 0.01$ , with an average modulus of  $1.389 \text{ kPa} \pm 0.289 \text{ kPa}$ , and displayed larger regional variations. It was also more viscous than gray matter and responded less rapidly to mechanical loading. Understanding the rheological differences between gray and white matter may have direct implications on diagnosing and understanding the mechanical environment in neurodevelopment and neurological disorders.

© 2015 Elsevier Ltd. All rights reserved.

\*Corresponding author at: Department of Mechanical Engineering, Stanford University, Stanford, CA 94305, USA. Tel.: +1 650 450 0855; fax: +1 650 725 1587.

E-mail address: [ekuhl@stanford.edu](mailto:ekuhl@stanford.edu) (E. Kuhl).

URL: <http://biomechanics.stanford.edu> (E. Kuhl).

## 1. Motivation

Our brain is not only our softest, but also our least well-understood organ. Floating in the cerebrospinal fluid, embedded in the skull, it is almost perfectly isolated from its mechanical environment (Miller, 2011). It is thus not surprising that most brain research focuses on the electrical rather than the mechanical characteristics of brain tissue (Chatelin et al., 2010). Recent studies suggest, though, that the mechanical environment plays an important role during neurodevelopment (Bayly et al., 2014). Mechanical factors are closely associated with developmental disorders including lissencephaly and polymicrogyria (Raybaud and Widjaja, 2011), reduced or increased brain folding (Budday et al., 2014), brachycephaly and plagiocephaly, flat or asymmetric heads (Hutchinson et al., 2004), and hydrocephalus, abnormal accumulation of cerebrospinal fluid (Franceschini et al., 2006).

Neuromechanics has traditionally displayed strong interest in the fast loading regime associated with dynamic phenomena on the order of seconds or milliseconds (Fallenstein et al., 1969). The prototype example is traumatic brain injury (Moore et al., 2009), where extreme loading rates cause intracranial damage associated with a temporary or permanent loss of function (Jérusalem and Dao, 2012). On these scales, time dependency plays a critical role (Prevost et al., 2011). Mathematical models for these phenomena naturally involve at least two time scales, one for the viscoelastic tissue and one for its poroelastic interaction with the cerebrospinal fluid (Chen and Bilston, 2007).

Neurodevelopment, on the contrary, falls into the slow loading regime associated with quasi-static phenomena on the order of weeks or months (Zilles et al., 2013). A typical example that has recently received growing attention is cortical folding (Sun and Hevner, 2014), where compressive forces between the gray matter layer and the white matter substrate cause structural instabilities and induce surface buckling (Budday et al., 2014). Mathematical models for these phenomena naturally involve at least two distinct materials, the gray matter layer with cell bodies, dendrites, and unmyelinated axons, and the white matter core with bundles of myelinated axons (Bayly et al., 2014).

To understand the mechanisms that drive neurodevelopment and trigger morphological abnormalities, it is critical to understand the rheological differences between gray and white matter tissue (Richman et al., 1975). Gyral wavelengths – and with them clinical markers such as gyrification indices – are directly correlated to the stiffness contrast between gray and white matter (Goriely et al., 2015). Controversies about the stiffness contrast have caused ongoing debate between the neuromechanics and neurobiology communities (Xu et al., 2010). While five decades of research have generated a profound understanding of brain tissue as a whole (Chatelin et al., 2010), the individual rheology of gray and white matter remains understudied and poorly understood. As a result of inconsistent sample preparation, post-mortem time, and testing conditions, reported stiffness values are often irreproducible and may vary by an order of magnitude or more (Miller, 2011): some studies reported that gray matter was substantially stiffer than white matter (Christ et al., 2010), others found that they were of equal

stiffness (Feng et al., 2013), and yet others observed that white matter was stiffer (van Dommelen et al., 2010). Here, to address this discrepancy, we adopt a robust, reliable, and repeatable method to quantify the mechanical properties of gray and white matter, flat-punch indentation. To systematically probe the sensitivity to indenter diameter, loading rate, holding time, post-mortem time, and location we perform a series of  $n = 192$  indentation tests. We demonstrate that indentation consistently produces robust measurements that indicate that white matter tissue is approximately one third stiffer than gray matter tissue.

## 2. Methods

### 2.1. Sample preparation

We collected fresh bovine brain of 16 months old cows from a local slaughterhouse (Martin's Custom Butchering, Wakarusa, IN). Within 2 h of post mortem, we prepared 5 mm-thick coronal slices for gray and white matter indentation. To slow down tissue degradation and prevent tissue dehydration, we hydrated the sample surfaces with phosphate-buffered saline solution and kept the slices refrigerated until testing. To exclude effects of neurofilament protein alteration and ensure tissue integrity, we performed all standard tests within 6 h post mortem (Fountoulakis et al., 2001). In addition, we tested one specimen repeatedly within five days post mortem to longitudinally characterize the effect of post-mortem time on gray and white matter mechanical properties. Fig. 1 illustrates the freshly harvested bovine brain, left, and a 5 mm-thick coronal slice prepared for indentation testing, right.

### 2.2. Experimental setup

We placed the fresh coronal slices in 100 mm-diameter petri dishes and stabilized the samples using a 12 mm-diameter stainless steel washer. To prevent specimen dehydration and minimize adhesion, we hydrated the surface inside the washer with phosphate-buffered saline solution before mounting the specimen into a Hysitron TI 950 TriboIndenter™ (Hysitron Inc., Eden Prairie, MN). Equipped with a three plate capacitive transducer, the TriboIndenter™ applies forces electrostatically at a resolution of  $< 1$  nN and simultaneously measures displacements as a change in capacitance at a resolution of  $< 0.02$  nm. We upgraded the standard TriboIndenter™ with an xZ 500 Extended Displacement Stage for soft matter testing to increase

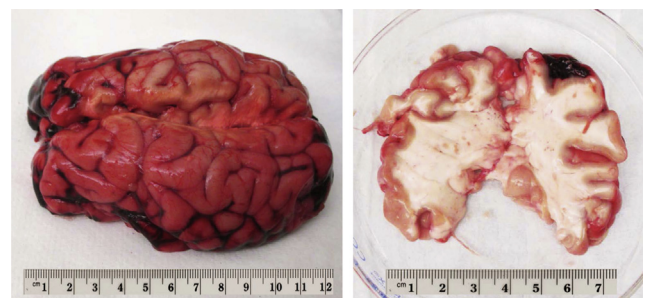


**Fig. 1** – Freshly harvested bovine brain, left, and 5 mm-thick coronal slice in petri dish prepared for indentation testing, right.



**Fig. 2 – Experimental setup.** A 5 mm-thick coronal slice of freshly harvested brain tissue is placed in a 100 mm-diameter petri dish and mounted underneath the force transducer of the TriboIndenter™. A 12 mm-diameter washer marks the indentation region and stabilizes the sample. A circular flat punch of 1.5 mm diameter ensures a homogenized specimen response.

the common range of indentation depths to 500  $\mu\text{m}$ . To ensure a homogeneous specimen response, we used circular flat punch indenters with diameters ranging from 0.75 mm to 1.50 mm. We fabricated the indenter tips from surface ground and polished tool steel, epoxied in a phenolic resin counterbored pin (Liu et al., 2009). Fig. 2 illustrates the experimental setup with the coronal slice mounted underneath the force transducer of the TriboIndenter™.

### 2.3. Indentation procedure

We performed all indentation tests at room temperature, with closed loop feedback at 78 kHz, under displacement control, using trapezoidal loading-holding-unloading profiles. We established two different loading protocols, single-long-range indentation and multiple-short-range indentation, and performed a series of  $n = 40$  long-range and  $n = 152$  short-range indentation tests. Fig. 3 illustrates the characteristic force-depth behavior of brain tissue during single-long-range indentation, black line, and multiple-short-range indentation, colored lines.

The single-long-range indentation protocol consists of a single indent with an indentation depth of 400  $\mu\text{m}$ , i.e., 8% of the specimen height, which lies within the recommended range of 10% to minimize boundary effects (Garo et al., 2007). Brain slices were not explicitly fixed to the petri dish, but stabilized with a washer; no significant sliding was observed between the slice and the dish. Loading and unloading rates are 5  $\mu\text{m}/\text{s}$  and the holding time is 10 s. Since this first protocol requires special equipment for long-range indentation and is relatively time consuming, we established an additional second test protocol for multiple-short-range indentation.

The multiple-short-range indentation protocol consists of four consecutive indents with an indentation depth of 10  $\mu\text{m}$ , i.e., 0.2% of the specimen height, applied at 300  $\mu\text{m}$  depth with increments of 10  $\mu\text{m}$ . Loading and unloading rates are 5  $\mu\text{m}/\text{s}$  and the holding time is 10 s. The recovery time between two consecutive indents is 120 s, which is more than twice the recommended recovery time of 50 s (van Dommelen et al., 2010).

We used the first protocol to gain a better understanding of the mechanical properties of gray and white matter in

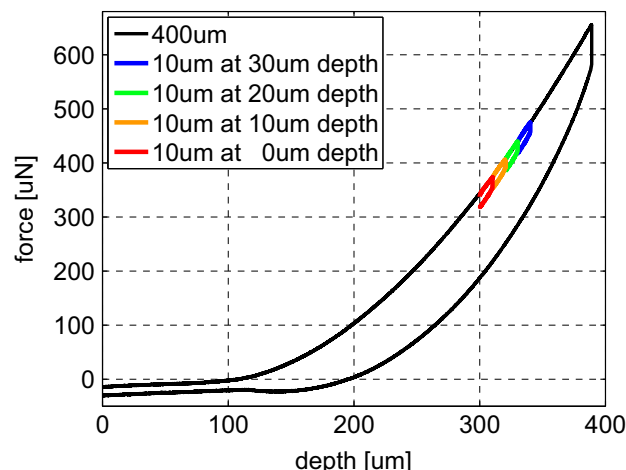


**Fig. 3 – Characteristic force-depth behavior during brain tissue indentation under displacement control.** The single-long-range indentation protocol consists of a single 400  $\mu\text{m}$ -deep indent, black line. The multiple-short-range indentation protocol consists of four consecutive 10  $\mu\text{m}$ -deep indents applied at 300  $\mu\text{m}$  depth with increments of 10  $\mu\text{m}$ , colored lines. The loading and unloading rates are 5  $\mu\text{m}/\text{s}$  and the holding time is 10 s.

general. To demonstrate our motivation for using a circular flat punch, we performed ten long-range indents in white matter tissue with varying punch diameters of 0.75 mm, 1.00 mm, 1.25 mm, and 1.50 mm. After this initial study, we performed all following indentations with the 1.50 mm-diameter punch. To illustrate the influence of the loading rate, we performed eight long-range indents in gray and white matter tissue with loading rates of 1  $\mu\text{m}/\text{s}$ , 2.5  $\mu\text{m}/\text{s}$ , 5  $\mu\text{m}/\text{s}$ , 10  $\mu\text{m}/\text{s}$ , 20  $\mu\text{m}/\text{s}$ , 40  $\mu\text{m}/\text{s}$ , 80  $\mu\text{m}/\text{s}$ , and 160  $\mu\text{m}/\text{s}$ . To illustrate the influence of the holding time, we performed eight long-range indents in white matter tissue with holding times of 1 s, 2.5 s, 5 s, 10 s, 20 s, 40 s, 80 s, and 160 s. We supplemented this series of relaxation tests by six long-term holding experiments with an expedited loading and unloading rate of 100  $\mu\text{m}/\text{s}$  and an extended holding time of 600 s, performed at three different locations in gray and white matter. Overall, this resulted in a series of  $n = 40$  long-range indentations,  $n = 10$  to characterize the sensitivity with respect to the punch diameter,  $n = 16$  to characterize the sensitivity with respect to the loading rate, and  $n = 14$  to characterize the sensitivity with respect to the holding time.

We used the second protocol to quantify the mechanical properties of bovine gray and white matter tissue. The second protocol is less invasive than the first, and also markedly faster, which allowed us to perform a series of systematic tests to characterize temporal and regional variations of gray and white matter moduli. To characterize temporal variations, we performed multiple-short-range indentation at the same spatial position in gray and white matter at ten different time points: 2 h, 3 h, 4 h, 6 h, 8 h, 10 h, 12 h, 1d, 2d, and 5d post mortem. To characterize regional variations, we performed multiple-short-range indentation immediately after slice preparation at 18 different spatial positions: at three different locations of three different coronal slices in both gray and white matter. Overall, this resulted in a series of  $n = 152$  short-range indentations,

$n = 80$  to characterize temporal variations and  $n = 72$  to characterize regional variations.

### 2.4. Mechanical properties

We defined the contact stiffness  $k$  of each indent as the average slope of the upper segment of the loading curve. To minimize the influence of adhesion (Gupta et al., 2007), we averaged the contact stiffness over the region between 50% and 100% of the maximum indentation force. The effective elastic modulus  $E_{\text{eff}}$  then follows directly from the standard relation (Oliver and Pharr, 2004),

$$E_{\text{eff}} = \frac{\sqrt{\pi}k}{2\sqrt{A}}, \quad (1)$$

where  $A$  is the projected contact area underneath the indenter. For a circular flat punch, the contact area,  $A = 1/4\pi d^2$ , is independent of the indentation depth and simply a function of the punch diameter  $d$ . This implies that the reduced elastic modulus simplifies to the following expression,

$$E_{\text{eff}} = \frac{k}{d}. \quad (2)$$

In general, the effective elastic modulus accounts for the elastic deformations in both sample and indenter (Oliver and Pharr, 2004),

$$\frac{1}{E_{\text{eff}}} = \frac{1-\nu_{\text{smp}}^2}{E_{\text{smp}}} + \frac{1-\nu_{\text{ind}}^2}{E_{\text{ind}}}, \quad (3)$$

where  $E_{\text{smp}}$  and  $E_{\text{ind}}$  are the Young's moduli and  $\nu_{\text{smp}}$  and  $\nu_{\text{ind}}$  are the Poisson's ratios of the sample and of the indenter. In our case, the stiffness of the indenter is orders of magnitude larger than the stiffness of the sample,  $E_{\text{ind}} \gg E_{\text{smp}}$ , and we can simplify this relation as follows:

$$E_{\text{smp}} = [1-\nu_{\text{smp}}^2]E_{\text{eff}} \quad (4)$$

Since our test setup does not allow us to directly quantify the compressive features of brain tissue, we adopt the common assumption of incompressibility,  $\nu_{\text{smp}} = 0.5$ , and simplify the sample modulus to following expression [11],

$$E_{\text{smp}} = \frac{3k}{4d}. \quad (5)$$

This implies that the gray and white matter moduli are directly proportional to the contact stiffness  $k$  and inversely proportional to the punch diameter  $d$ . To test this hypothesis, we measured the contact stiffness  $k$  at a constant, fixed location using circular flat punches of varying diameters  $d$  to ensure that our method reliably records constant sample moduli  $E_{\text{smp}}$ .

## 3. Results

### 3.1. General indentation characteristics

Fig. 3 displays the general indentation characteristics of brain tissue under single-long-range and multiple-short-range indentation. For the single-long-range indentation, we chose the starting position of the indenter tip 100  $\mu\text{m}$  above the sample surface to guarantee that the initial setup is contact-free. We then gradually increased the indentation depth. At first, we recorded a small negative force resulting from

adhesive forces between the indenter tip and the hydrated sample surface. With increasing indentation depth, the tip gradually came in contact with the sample and the recorded force began to increase. Eventually, the resistance of the sample balanced the adhesive forces and the total force vanished. Then the force increased gradually until the tip surface was in full contact with the sample. From this point onward, the force recording was stable; the force-depth relation was initially slightly strain stiffening, but then almost linear. At a maximum indentation depth of 400  $\mu\text{m}$ , we held the indentation depth constant, and the force decreased upon relaxation. We then gradually decreased the indentation depth and the force decreased accordingly. Towards the end of the unloading regime, the recorded force temporarily dropped below zero indicating adhesive effects, until it finally recovered its initial value. Since single-long-range indentation required extended recovery times, we used it primarily to calibrate the method and then switched to multiple-short-range indentation to perform repeated tests for gray and white matter characterization. To ensure a linear response during short-range indentation, we performed four consecutive indents with an indentation depth of 10  $\mu\text{m}$  at depth increments of 10  $\mu\text{m}$ . The colored curves in Fig. 3 confirm that the behavior during these four indents was indeed linear and lay well within the linear regime of the black single long-range indentation curve.

### 3.2. Indenting with a circular flat punch

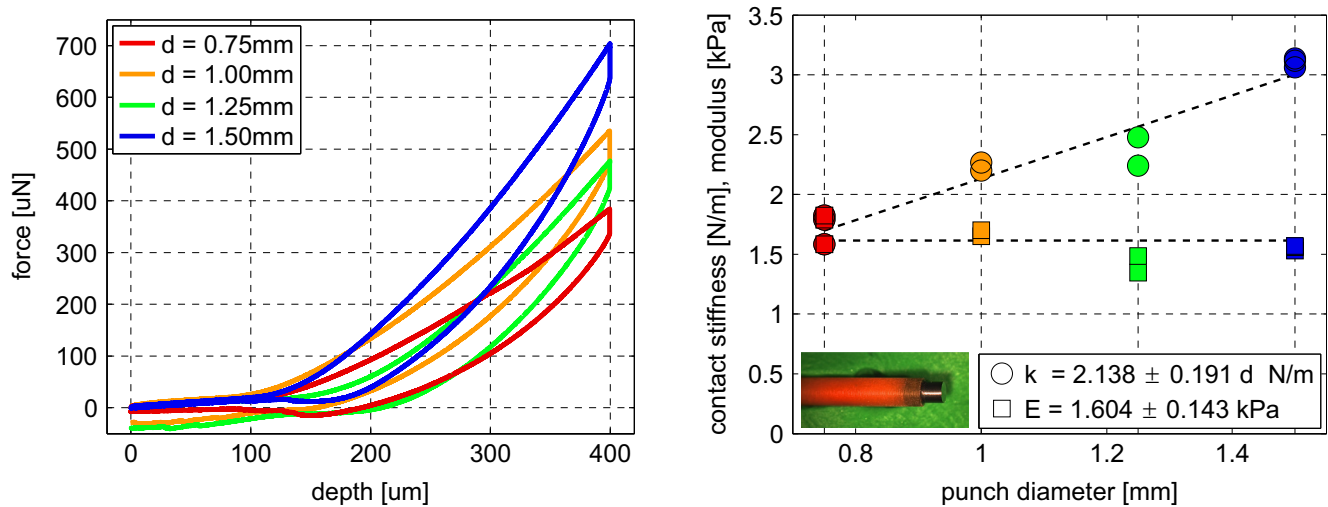
Fig. 4 illustrates the tissue response when varying the diameter of the indenter. To ensure that our method reliably records constant sample moduli, we performed a series of ten single-long-range indents in white matter tissue with varying punch diameters of 0.75 mm, 1.00 mm, 1.25 mm, and 1.50 mm.

Fig. 4, left, shows that the contact stiffness, the slope of the force-depth curve, increased with increasing punch diameter, from  $1.732 \pm 0.129$  N/m at a diameter of 0.75 mm via  $2.233 \pm 0.048$  N/m at a diameter of 1.00 mm and  $2.359 \pm 0.167$  N/m at a diameter of 1.25 mm to  $3.106 \pm 0.038$  N/m at a diameter of 1.50 mm. Fig. 4, right, illustrates the linear relation between contact stiffness and punch diameter with a slope of  $2.138 \pm 0.191$  N/m d. This confirms our initial hypothesis that the specimen modulus is directly proportional to the contact stiffness and inversely proportional to the punch diameter, here with a factor of  $1.604 \pm 0.143$  kPa. From now on, we performed all remaining indentations with the 1.50 mm-diameter punch illustrated in Fig. 4.

### 3.3. Mechanical properties of gray and white matter

Figs. 5 and 6 illustrate the loading rate sensitivity of gray and white matter. To explore the rate-dependent nature of brain tissue, we performed a series of 16 single-long-range indents, eight in gray and eight in white matter, at eight different loading rates of 1  $\mu\text{m/s}$ , 2.5  $\mu\text{m/s}$ , 5  $\mu\text{m/s}$ , 10  $\mu\text{m/s}$ , 20  $\mu\text{m/s}$ , 40  $\mu\text{m/s}$ , 80  $\mu\text{m/s}$ , and 160  $\mu\text{m/s}$ .

Fig. 5 shows that for a displacement-controlled trapezoidal loading-holding-unloading profile, the indentation force increased gradually towards its maximum value, then decayed quickly during holding, and finally decreased towards zero. The maximum indentation force increased markedly with increasing



**Fig. 4 – Variation of punch diameter. Sensitivity of indentation force vs. indentation depth for circular flat punches with different diameter reveals a linear relation between contact stiffness and punch diameter. The slope of the force–depth curve increases with increasing punch diameter, left. The contact stiffness increases linearly with increasing punch diameter and the sample modulus is constant.**

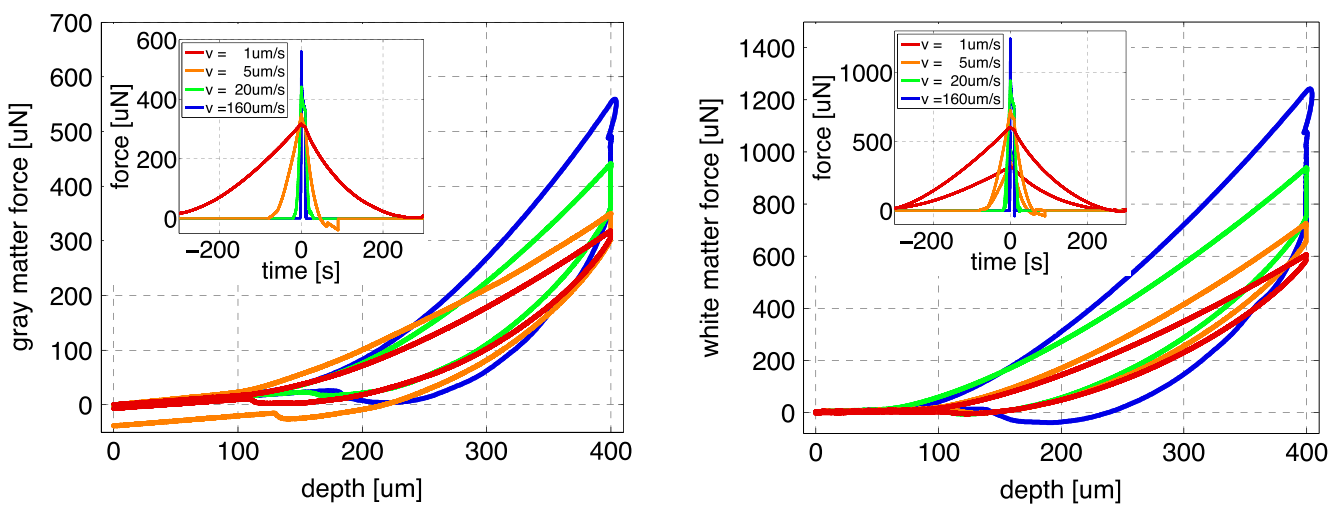


**Fig. 5 – Loading rate sensitivity of gray and white matter. Sensitivity of indentation force vs. indentation depth for varying loading rates reveals the rate dependent nature of brain tissue. Indentation force and modulus increase with increasing loading rate.**

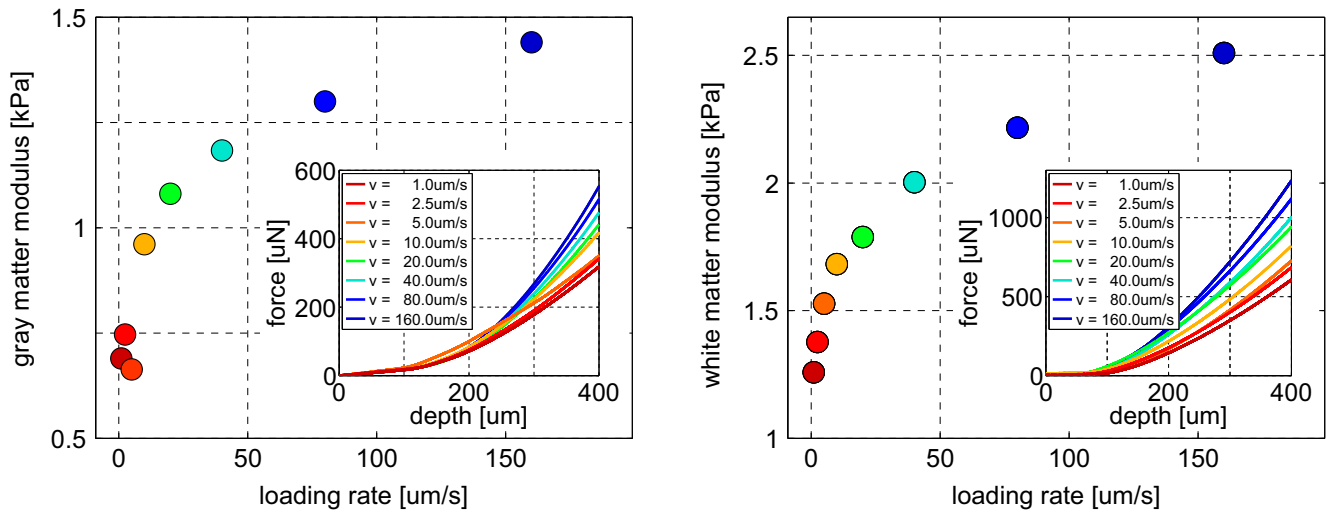
loading rate. Within our analyzed velocity range from  $1 \mu\text{m/s}$  to  $160 \mu\text{m/s}$ , the maximum force in gray matter increased from  $318 \mu\text{N}$  to  $559 \mu\text{N}$  and the maximum force in white matter increased from  $605 \mu\text{N}$  to  $1242 \mu\text{N}$ . Both gray and white matter approximately doubled their maximum forces when increasing the loading rate by two orders of magnitude.

Fig. 6 illustrates the gray and white matter force–depth behavior and the corresponding moduli throughout the entire loading rate spectrum. Maximum forces and moduli increased with increasing loading rate. Within our analyzed loading rate regime from  $1 \mu\text{m/s}$  to  $160 \mu\text{m/s}$ , the gray matter modulus increased from  $0.689 \text{ kPa}$  to  $1.440 \text{ kPa}$  and the white matter modulus increased from  $1.259 \text{ kPa}$  to  $2.510 \text{ kPa}$ . Both gray and white matter doubled their moduli when increasing the loading rate by two orders of magnitude. From now on,

we performed all remaining indentations at loading and unloading rates of  $5 \mu\text{m/s}$  to reduce loading rate sensitivity and tissue preservation time.

Figs. 7 and 8 illustrate the holding time sensitivity of gray and white matter. To explore the rate-dependent nature of brain tissue, we performed eight single-long-range indents in white matter tissue with holding times of 1 s, 2.5 s, 5 s, 10 s, 20 s, 40 s, 80 s, and 160 s and an additional six relaxation tests with extended holding times of 600 s in gray and white matter, at three different locations each.

Fig. 7 illustrates the increase in relaxation force for increasing holding times and summarizes the individual relaxation tests in a single characteristic relaxation curve. The curve shows that the total stress decreased rapidly with increasing holding time and then converges gradually towards its static equilibrium value.



**Fig. 6 – Loading rate sensitivity of gray and white matter. Sensitivity of indentation force vs. indentation depth for varying loading rates reveals the rate dependent nature of brain tissue. Indentation force and modulus increase with increasing loading rate.**

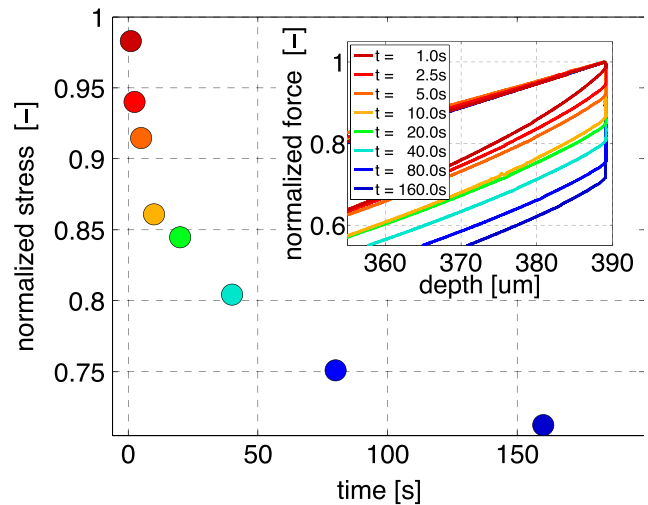
Within our analyzed holding range from 1 s to 160 s, the normalized stress decreased from 0.983 to 0.712, i.e., it reduced its initial value by more than one fourth.

Fig. 8 illustrates the characteristic stress relaxation behavior of gray and white matter. To quantify the viscoelastic response, we adopted a multi-term Prony series,  $\sigma(t) = \sigma_\infty + [\sigma_i - \sigma_\infty] \sum_{i=1}^n \exp(-t/\tau_i)$ , with  $n$  characteristic time constants  $\tau_i$ . The plateau stress  $\sigma_\infty$  at  $t \rightarrow \infty$  is associated with the storage modulus and mimics the elastic response; the difference between peak stress and plateau stress  $[\sigma_i - \sigma_\infty]$  is associated with the loss modulus and mimics the viscoelastic response. We found the best approximation for a two-term Prony series.

Table 1 summarizes the two time constants  $\tau_1$  and  $\tau_2$  for gray and white matter. The short and long time scales of both gray and white matter differed by almost two orders of magnitude: White matter, with a fast time constant of  $\tau_1 = 4.40 \pm 0.22$  s, responded equally fast to loading as gray matter, with a fast time constant of  $\tau_1 = 4.24 \pm 0.59$  s. White matter, with a slow time constant of  $\tau_2 = 160.74 \pm 18.37$  s, displayed slightly longer relaxation times than gray matter, with a slow time constant of  $\tau_2 = 105.74 \pm 50.97$  s. This slower response of white matter is clearly visible in the relaxation curves of Fig. 8, in which the gray matter stress plateaued within the 600 s time interval, while the white matter stress still decayed beyond 600 s. From now on, we performed all remaining indentations with holding times of 10 s to reduce both experimental time and preservation time.

### 3.4. Temporal variation of gray and white matter properties

Figs. 9 and 10 and Table 2 summarize the temporal evolution of the gray and white matter moduli for different indentation times post mortem. To characterize the impact of tissue preservation on the mechanical response, we performed multiple-short-range indentations at the identical spatial position in gray and white matter at ten different time points, 2 h, 3 h, 4 h, 6 h, 8 h, 10 h, 12 h, 1d, 2d, and 5d post mortem.



**Fig. 7 – Holding time sensitivity of white matter. Sensitivity of relaxation force vs. indentation depth for varying holding times reveals the rate dependent nature of brain tissue. The relaxation force increases for increasing holding times. The total stress decreases for increasing holding times and converges asymptotically towards its plateau value.**

Fig. 9 illustrates the force-depth response of gray and white matter tissue on days d0, d1, d2, and d5 post mortem. The consistent shape of the indentation curves indicates that, when kept intact and hydrated, brain slices were virtually insensitive to the time of preservation. Within our analyzed time interval, the gray matter modulus varied between 1.063 kPa on day 0, 1.131 kPa on day 1, 1.065 kPa on day 2, and 1.175 kPa on day 5, and the white matter modulus varied between 1.966 kPa on d0, 1.860 kPa on day 1, 1.849 on day 2, and 1.979 kPa on day 5. The indentation force in white matter, right, was consistently larger than in gray matter, left.

Fig. 10 illustrates the temporal variation of the gray and white matter moduli within five days post mortem. The

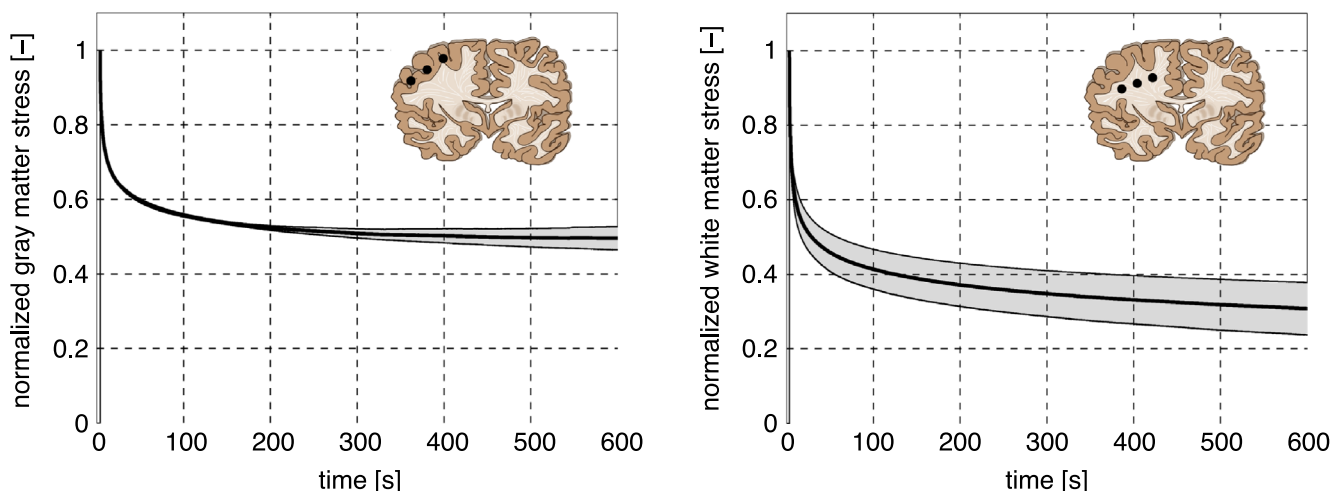


**Fig. 8 – Stress relaxation of gray and white matter. Individual relaxation tests reveal the rate dependent nature of brain tissue. The plateau stress is associated with the storage modulus and characterizes the elastic response; the difference between peak stress and plateau stress is associated with the loss modulus and characterizes the viscoelastic response. Black curves indicate the mean; gray zones indicate the standard deviation.**

**Table 1 – Stress relaxation of gray and white matter. Least squares fit reveal the best approximation for a two-term Prony series suggesting that brain tissue possesses two characteristic time scales  $\tau_1$  and  $\tau_2$ .**

Indent	Gray matter (s)			mean	$\pm$	std
	I1	I2	I3			
$\tau_1$	4.08	4.90	3.75	4.24	$\pm$	0.59
$\tau_2$	71.24	164.29	81.70	105.74	$\pm$	50.97
Indent	White matter (s)			mean	$\pm$	std
	I1	I2	I3			
$\tau_1$	4.63	4.38	4.20	4.40	$\pm$	0.22
$\tau_2$	139.81	174.22	168.18	160.74	$\pm$	18.37

dashed vertical lines highlight the moduli at days d0, d1, d2 and d5 corresponding to the curves in Fig. 9. Both gray and white matter moduli consistently increased with the number of indents and increasing indentation depths. Both gray and white matter moduli varied moderately during the first day of repeated mechanical testing, but displayed consistent moduli when tested after long periods of rest at d0, d1, d2, and d5. Throughout all ten time points, gray matter, left, was consistently softer than white matter, right. White matter, with an average modulus of  $1.877 \pm 0.145$  kPa, was stiffer than gray matter, with an average modulus of  $1.216 \pm 0.124$  kPa. Standard deviations in white and gray matter moduli were 8% and 10%. When restricting averaging to the rested tissue samples from d0, d1, d2, and d5 in Fig. 9 alone, i.e., when excluding the measurements from 3 h, 4 h, 6 h, 8 h, 10 h, 12 h post mortem, for which the sample had possibly not fully recovered, the average white and gray matter moduli were  $1.913 \pm 0.104$  kPa and  $1.108 \pm 0.055$  kPa, with even lower standard deviations of 5% in both gray and white matter. Table 2 summarizes the gray and white matter moduli for all  $n = 80$  short-range indentations. From now on, we performed all remaining

indentations within 6 h post mortem to reduce tissue preservation time.

### 3.5. Regional variation of gray and white matter properties

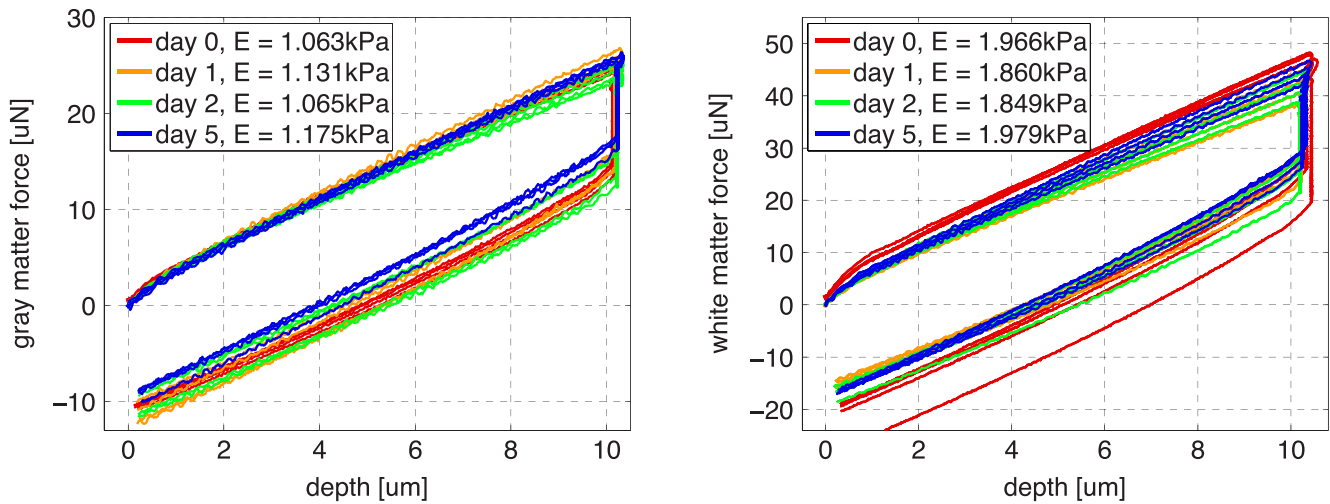
Fig. 11 and Table 3 summarize the regional variations of gray and white matter properties. To characterize regional variations, we performed multiple-short-range indentations at 18 different spatial positions within 6 h post mortem, at three different locations of three different coronal slices in both gray and white matter.

Fig. 11 illustrates the regional variation of the specimen moduli at nine locations in gray and nine locations in white matter. Both gray and white matter moduli consistently increased with the number of indents and increasing indentation depths. White matter, with an average modulus of  $1.895 \pm 0.592$  kPa, was on average 39% stiffer than gray matter,  $p < 0.01$ , with an average modulus of  $1.368 \pm 0.289$  kPa. White matter, with a standard deviation of 31%, displayed stronger regional variations than gray matter, with a standard deviation of 21%. Table 3 summarizes the gray and white matter moduli for all  $n = 72$  short-range indentations.

## 4. Discussion

### 4.1. General indentation characteristics

Despite intense efforts towards characterizing the mechanical properties of brain tissue, the rheological differences between gray and white matter remain poorly understood. Reported gray and white matter moduli differ by an order of magnitude and more, mainly because of inconsistencies in sample preparation, post-mortem time, and testing conditions (Miller, 2011). The extremely soft nature and the small sample size make standard rheological testing challenging and only a few techniques are capable of truly distinguishing between gray



**Fig. 9 – Temporal variation of gray and white matter indentation force on at four different depths at days d0, d1, d2, and d5 post mortem. The consistent shape of the indentation curves reveals that brain slices are virtually insensitive to the time of preservation. The indentation force in gray matter, left, is consistently lower than white matter, right.**

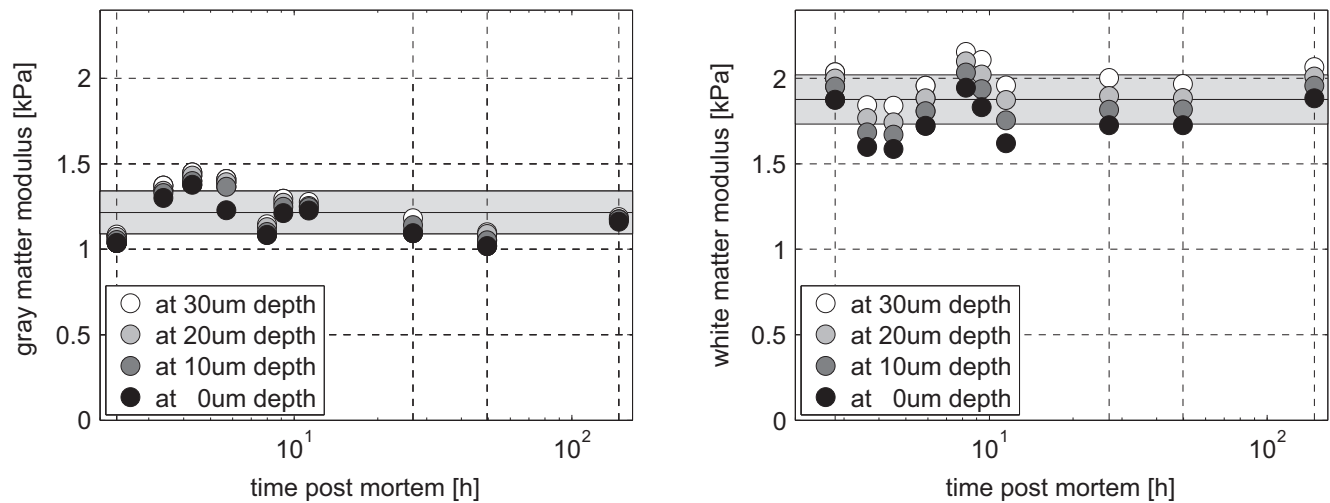


**Fig. 10 – Temporal variation of gray and white matter moduli. The consistent moduli within five days post mortem reveal that brain slices are virtually insensitive to the time of preservation. The stiffness increases moderately with indentation depth, from black dots to white dots. Gray matter, left, is consistently softer than white matter, right. Black horizontal lines indicate the mean; gray zones indicate the standard deviation.**

and white matter properties (Chatelin et al., 2010). Here we established an easy-to-use protocol to robustly, reliably, and reproducibly test gray and white matter brain tissue. To illustrate the features of this method, we performed a series of  $n = 192$  indentation tests of freshly harvested bovine brain,  $n = 40$  long-range indentations to establish our protocols and calibrate our method and  $n = 152$  short-range indentations to characterize temporal and regional variations. Indentation testing for various indenter diameters, loading rates, holding times, post-mortem times, and locations consistently produced robust results.

#### 4.2. Indenting with a circular flat punch

A common challenge when indenting soft biological tissue is that, in contrast to stiff materials such as bone (Zhang

et al., 2010), adhesion can significantly alter the contact area beneath the indenter and induce errors in the mechanical characterization (Kohn and Ebenstein, 2013). To address this issue, we used a circular flat punch (Liu et al., 2009) instead of the commonly used spherical indenter (Gefen and Margulies, 2004; Gupta et al., 2007; van Dommelen et al., 2010). Using custom-designed indenter tips with four different diameters, we have shown that in flat-punch indentation, the contact area between indenter and sample remains constant over wide ranges of indentation depths (Blum and Ovaert, 2012). This implies that the specimen modulus  $E_{\text{cmp}} = 3/4 k/d$  is directly proportional to the contact stiffness  $k$  and inversely proportional to the punch diameter  $d$ , independent of the indentation depth (Liu et al., 2009). Our linear force-depth response during multiple-short-range indentation in Figs. 3

and 9 confirms this hypothesis. Our gray and white matter moduli agree with those derived in 1.50 mm-diameter circular flat punch indentation of porcine brain, which,

however, required a complex finite-element based analysis to determine the specimen moduli  $E_{\text{smpl}}$  from the measured contact stiffnesses  $k$  (Kaster et al., 2011).

**Table 2 – Temporal variation of gray and white matter moduli. Measurements at ten time points, rows, for four consecutive indentations, columns, with indentation depths of 10  $\mu\text{m}$  at increments of 10  $\mu\text{m}$ , tested within five days post mortem.**

Indent	Gray matter moduli (kPa)							Indent	White matter moduli (kPa)						
	I1	I2	I3	I4	mean	$\pm$	std		I1	I2	I3	I4	mean	$\pm$	std
2 h	1.037	1.054	1.072	1.087	1.063	$\pm$	0.021	2 h	1.875	1.951	1.999	2.036	1.966	$\pm$	0.070
3 h	1.301	1.329	1.342	1.372	1.336	$\pm$	0.030	3 h	1.598	1.683	1.767	1.843	1.723	$\pm$	0.106
4 h	1.377	1.400	1.431	1.450	1.414	$\pm$	0.032	4 h	1.587	1.671	1.743	1.839	1.710	$\pm$	0.107
6 h	1.228	1.366	1.393	1.410	1.349	$\pm$	0.083	6 h	1.723	1.809	1.883	1.957	1.843	$\pm$	0.100
8 h	1.085	1.101	1.130	1.146	1.115	$\pm$	0.028	8 h	1.946	2.034	2.100	2.154	2.059	$\pm$	0.090
10 h	1.212	1.249	1.271	1.296	1.257	$\pm$	0.036	10 h	1.832	1.937	2.023	2.108	1.975	$\pm$	0.118
12 h	1.227	1.248	1.253	1.278	1.251	$\pm$	0.021	12 h	1.620	1.754	1.873	1.960	1.802	$\pm$	0.147
1 d	1.095	1.142	1.104	1.181	1.131	$\pm$	0.039	1 d	1.727	1.816	1.897	2.002	1.860	$\pm$	0.117
2 d	1.019	1.053	1.089	1.099	1.065	$\pm$	0.037	2 d	1.726	1.819	1.884	1.967	1.849	$\pm$	0.102
5 d	1.161	1.174	1.177	1.188	1.175	$\pm$	0.011	5 d	1.883	1.958	2.011	2.065	1.979	$\pm$	0.078
mean	1.174	1.211	1.226	1.251	1.216			mean	1.752	1.843	1.918	1.993	1.877		
$\pm$ std	0.116	0.127	0.131	0.130		$\pm$	0.124	$\pm$ std	0.128	0.123	0.114	0.103		$\pm$	0.145

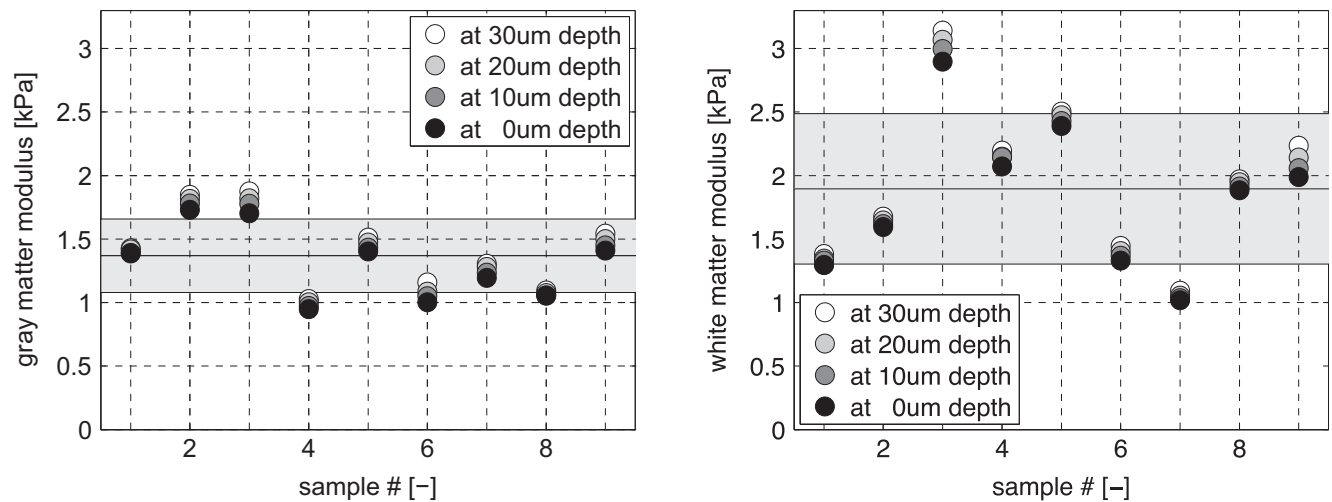


**Fig. 11 – Regional variation of gray and white matter moduli. Measurements at three different slices and three different locations reveal that the specimen moduli vary markedly across the brain. Gray matter, left, is softer than white matter, right, and displays smaller regional variations. Black horizontal lines indicate the mean; gray zones indicate the standard deviation.**

**Table 3 – Regional variation of gray and white matter moduli. Measurements at nine different locations, rows, for four consecutive indentations, columns, with indentation depths of 10  $\mu\text{m}$  at increments of 10  $\mu\text{m}$ , tested within 6 h post mortem.**

Indent	Gray matter moduli (kPa)							Indent	White matter moduli (kPa)						
	I1	I2	I3	I4	mean	$\pm$	std		I1	I2	I3	I4	mean	$\pm$	std
#1	1.386	1.392	1.419	1.428	1.406	$\pm$	0.020	#1	1.295	1.329	1.347	1.381	1.338	$\pm$	0.036
#2	1.730	1.780	1.816	1.848	1.794	$\pm$	0.051	#2	1.594	1.617	1.647	1.676	1.633	$\pm$	0.036
#3	1.702	1.777	1.820	1.874	1.794	$\pm$	0.072	#3	2.896	2.996	3.068	3.141	3.025	$\pm$	0.104
#4	0.948	0.974	1.001	1.028	0.988	$\pm$	0.035	#4	2.071	2.145	2.148	2.197	2.140	$\pm$	0.052
#5	1.403	1.431	1.473	1.510	1.454	$\pm$	0.047	#5	2.390	2.429	2.474	2.504	2.449	$\pm$	0.050
#6	1.004	1.051	1.087	1.158	1.075	$\pm$	0.065	#6	1.331	1.369	1.405	1.445	1.387	$\pm$	0.049
#7	1.194	1.236	1.281	1.304	1.254	$\pm$	0.049	#7	1.018	1.035	1.055	1.093	1.050	$\pm$	0.032
#8	1.054	1.057	1.075	1.095	1.070	$\pm$	0.019	#8	1.883	1.914	1.946	1.970	1.928	$\pm$	0.038
#9	1.410	1.451	1.499	1.542	1.476	$\pm$	0.058	#9	1.987	2.058	2.142	2.234	2.105	$\pm$	0.107
mean	1.314	1.350	1.386	1.421	1.368			mean	1.830	1.877	1.915	1.960	1.895		
$\pm$ std	0.287	0.299	0.304	0.307		$\pm$	0.289	$\pm$ std	0.590	0.612	0.627	0.638		$\pm$	0.592

#### 4.3. Elastic properties of gray and white matter

Our study suggests that white matter displays higher maximum indentation forces and steeper indentation curves than gray matter as illustrated in Figs. 5 and 6. White matter, with a modulus of 1.895 kPa, was on average 36% stiffer than gray matter, with a modulus of 1.389 kPa. This stiffness difference is microstructurally plausible since white matter consists primarily of myelinated axons (Holland et al., 2015), which act as a network of biopolymer filaments (Holzapfel and Ogden, 2013), while gray matter is largely composed of cell bodies. Contrary to the common belief that biofilaments are non-load-bearing under compression, recent studies have shown that biofilaments contribute notably to the compressive load carrying capacity of soft tissues (Böl et al., 2014). Only one indentation study found opposite results and reported that white matter, with a modulus of 0.294 kPa, was softer than gray matter, with a modulus of 0.454 kPa, using atomic force microscopy on ultra thin rodent brain slices (Christ et al., 2010). Other studies of porcine brain agreed favorably with our measurements and reported an average stiffness difference of 39% between white matter, with 3.083 kPa, and gray matter, with 2.223 kPa (van Dommelen et al., 2010). These moduli are overall 60% stiffer than ours, but were also recorded at higher loading rates. Our measurements agree closely with the white and gray matter moduli of 1.787 kPa and 1.195 kPa for porcine brain, found by indenting 10 mm-thick slices at a depth of 160  $\mu\text{m}$  (Kaster et al., 2011). In contrast to our method, however, this study required complex finite-element analyses to evaluate the relationship between specimen modulus and contact stiffness.

#### 4.4. Viscoelastic properties of gray and white matter

Variations in loading rate and holding time illustrated in Figs. 5–8 reveal the extreme rate-sensitivity of brain tissue (Galford and McElhaney, 1970). White matter was as loading-rate sensitive as gray matter. Both doubled their maximum indentation forces, and with them their moduli, when increasing the loading rate by two orders of magnitude as illustrated in Figs. 5 and 6. This agrees well with split Hopkinson pressure bar compression tests, which reported increasing moduli with increasing loading rate in bovine brain samples (Pervin and Chen, 2009). Similar to our study, this study found that white matter was consistently stiffer than gray matter. However, since this study was motivated by understanding brain mechanics during traumatic brain injury, it focused on the fast-loading-rate regime. Here, since we are interested in understanding brain mechanics during brain development, we focused on the slow-loading-rate regime (Garcia et al., 2012). Our loading rates are comparable to the medium loading rates in early compression tests (Miller and Chinzei, 1997) and to the slow loading rates in recent indentation tests (van Dommelen et al., 2010). Our findings are in general agreement with the literature, where the specimen modulus increased with increasing loading rate (Chatelin et al., 2010; Miller and Chinzei, 1997; van Dommelen et al., 2010).

White matter, with a stress relaxation of 70% and relaxation times larger than 600 s, was more viscous and responded more slowly than gray matter, with a stress relaxation of 50% and relaxation times of 400 s. This rheological difference is closely related to the microstructural architecture of gray and

white matter tissue and reflects the network properties of white matter, similar to filled elastomers (Franceschini et al., 2006). This is in agreement with recent studies, which have explained macroscopic viscoelasticity with the intracellular interaction between cytoplasm, nucleus, and membrane during cellular deformation (Jérusalem and Dao, 2012). Our long-time relaxation curves in Fig. 8, right, with white matter plateau stresses of  $\sigma_\infty/\sigma_0 < 0.30$  and relaxation times larger than 600 s, agree both qualitatively and quantitatively with the white matter relaxation curves reported in the literature, for which the stresses decayed to  $\sigma_\infty/\sigma_0 < 0.30$  and had still not fully converged after 500 s (Chen and Bilston, 2007). Our larger but slower drop in white matter stress agrees with the recently reported larger but slower drop in white matter stiffness when compared to gray matter (van Dommelen et al., 2010).

We found that a first-order viscoelastic model,  $\sigma(t) = \sigma_\infty + [\sigma_0 - \sigma_\infty] \exp(-t/\tau)$ , underestimated early relaxation and overestimated late relaxation. This suggests that a first-order viscoelastic model might be too simplistic to characterize the complex rate-dependent nature of brain tissue. Several authors have suggested to use a Prony series with additional terms,  $\sigma(t) = \sigma_\infty + \sum_{i=1}^n [[\sigma_0 - \sigma_\infty] \exp(-t/\tau_i)]$ , to capture the different time scales of brain tissue (Miller and Chinzei, 1997). While some authors suggest that a two-term model provides a sufficiently accurate fit (Gefen and Margulies, 2004; Prange and Margulies, 2002), others prefer a three-term model, either plain (Elkin and Morrison, 2013; Tamura et al., 2007), or in combination with the cerebrospinal fluid in a poroviscoelastic formulation (Chen and Bilston, 2007).

We found that a second-order Prony series,  $\sigma(t) = \sigma_\infty + [\sigma_0 - \sigma_\infty] \exp(-t/\tau_1) + [\sigma_0 - \sigma_\infty] \exp(-t/\tau_2)$ , with two time scales  $\tau_1$  and  $\tau_2$  provided an accurate approximation of both early and late relaxation. The characteristic time scales differed by almost two orders of magnitude for both gray and white matter. From a rheological point of view, this suggests that one time scale could be associated with the viscous and one with the porous nature of brain tissue. Including porous effects seems particularly important when modeling the interplay between early and late relaxation at high loading rates (Lang et al., 2014), which was beyond the scope of the current study.

#### 4.5. Temporal variation of gray and white matter properties

Our study suggests that when kept intact and hydrated, thick brain slices can be preserved over periods of days without significant alteration in mechanical properties. To prevent specimen dehydration, rather than bathing the entire sample, we only hydrated the specimen surface to reduce the effects of osmotic swelling and long-term water evaporation in the near-surface region (Miller, 2011). Inherent advantages of testing thick, structurally intact brain slices, rather than small cylindrical (Franceschini et al., 2006), disc-shaped (Pervin and Chen, 2009) or cuboid (Prange and Margulies, 2002; van Dommelen et al., 2010) specimens, are that larger structural dimensions naturally minimize dehydration, swelling, structural degradation, and boundary effects (Miller, 2011). Because of boundary effects, traditional consolidation tests on brain samples can be challenging (Chen and Bilston, 2007). In practice, unconfined

compression is often used as an approximation to calibrate the poroviscoelastic properties of brain tissue (Franceschini et al., 2006). Since our indentation of thick brain slices is inherently local, it closely mimics the in situ environment and naturally provides realistic lateral confinement conditions for both solid deformation and fluid flow.

Our study revealed that both gray and white matter tissue are insensitive to preservation times. From systematic post-mortem reports of protein level alterations, we know that 6 h after death, brain tissue displays noticeable signs of proteolysis, a possible indicator for structural degradation (Fountoulakis et al., 2001). Oscillatory shear tests of freshly harvested porcine brain samples revealed a marked increase in tissue stiffness starting 6 h post mortem (Garo et al., 2007). However, these studies were performed upon continued mechanical loading. Here, we minimized exposure to mechanical testing to clearly separate the effects of mechanical history and post-mortem time. When comparing frequently tested specimens on the first day post mortem, gray and white matter moduli displayed standard deviations of 13% and 16% as summarized in Fig. 10 and Table 2. When comparing rested and recovered specimens within five days post mortem, standard deviations in both gray and white matter moduli were as low as 5% as indicated in Figs. 9 and 10. Early findings from almost half a decade ago reported that the mechanical properties of live, dead, and fixed mammalian brain tissue were virtually indistinguishable (Metz et al., 1970). A comparison of in vivo, in situ, and in vitro tissue properties confirmed these observations, and suggested that perfusion does not affect the stiffness of living brain tissue (Gefen and Margulies, 2004).

Both gray matter and white matter moduli consistently increased with the number of indentation cycles during multiple-short-range indentation as highlighted in Fig. 10 and Table 2. This is in agreement with the reported structural stiffening upon preconditioning, an effect that disappeared after five to six cycles (Gefen and Margulies, 2004). Our results suggest that the effect of preconditioning is fully reversible within a few hours of rest. In summary, the mechanical history of the specimen might play a more important role than previously assumed (Prevost et al., 2011): The recommended rest period of 50 s between two consecutive tests might seriously underestimate the necessary recovery time, especially when testing at low loading rates for long testing times (van Dommelen et al., 2010).

#### 4.6. Regional variation of gray and white matter properties

Our study indicates that white matter, with an average modulus of  $1.895 \text{ kPa} \pm 0.592 \text{ kPa}$ , was on average 39% stiffer than gray matter, with an average modulus of  $1.368 \text{ kPa} \pm 0.289 \text{ kPa}$ , as illustrated in Fig. 11. A two-sample t-test revealed a significant difference in white and gray matter stiffness,  $p < 0.01$ . White matter, with a standard deviation of 31%, displayed stronger regional variations than gray matter, with a standard deviation of 21%, as indicated in Table 3. Various studies have shown that brain tissue properties do indeed

display a strong regional variation (Chatelin et al., 2010). Our trends are in agreement with the recent literature and suggest that the microstructural architecture of white matter is more heterogeneous than gray matter, and also more anisotropic (van Dommelen et al., 2010).

#### 4.7. Limitations

Our current study focused on characterizing the differences between gray and white matter tissue. We are currently enhancing our model to characterize tissue nonlinearities in the large deformation regime. We are also performing dynamic testing to characterize storage and loss moduli for different frequencies (Miller, 2011) and compare the results to the quasi-static relaxation tests reported here. This will allow us to better characterize the time-dependent behavior, and, possibly, by using inverse finite element analysis (Böl et al., 2013), to correlate it closely to a poroviscoelastic material model (Franceschini et al., 2006). Since the present study was initially motivated by the long time scales of brain development (Franze et al., 2013), nonlinearities and short time scales were less relevant here.

While our indentation method reliably recorded gray and white matter moduli, it remains an ex vivo technique that cannot predict the mechanical characteristics of living brain tissue in situ. Within the past decade, magnetic resonance elastography has rapidly advanced as a non-invasive, in vivo tool, directly applicable to living human brain tissue (Hamhaber et al., 2007). Magnetic resonance elastography measures the mechanical properties of soft tissues by introducing shear waves and assessing their propagation velocity using magnetic resonance imaging. A recent study in ferrets suggested that, at loading rates from 400 Hz to 800 Hz, elastic and viscous properties of gray and white matter were indistinguishable (Feng et al., 2013). Another study in humans at loading rates of 200 Hz found that gray matter storage moduli, with 3.1 kPa, were on average 12% larger than white matter storage moduli, with 2.7 kPa, while loss moduli of gray and white matter, with 2.5 kPa, were identical (Green et al., 2008). This is in strong disagreement with another magnetic resonance elastography study in humans, which found that white matter moduli, with 40.8 kPa, were on average 161% larger than the gray matter moduli, with 15.6 kPa (Kruse et al., 2008). Despite its tremendous potential, magnetic resonance elastography data seem to vary markedly, both qualitatively and quantitatively, mainly because the technology itself is still in its infancy (Chatelin et al., 2010).

---

## 5. Concluding remarks

We have presented an easy-to-use, robust, reliable, and repeatable method to characterize the mechanical properties of gray and white matter tissue. To probe coronal slices of fresh mammalian brain, we used a commercially available nanoindentation instrument, initially designed for stiff inorganic materials, and replaced its commonly used sharp indenter tip with a circular flat punch. Flat-punch indentation of thick, intact brain slices minimizes adhesion effects and other challenges associated with small specimens and

naturally minimizes boundary effects, dehydration, swelling, and structural degradation. Our coronal slices maintained their structural integrity within five days post mortem, and their mechanical properties remained virtually unchanged: white matter was approximately one third stiffer than gray matter and displayed larger regional variations; it was more viscous than gray matter and displayed longer relaxation times. Understanding the rheological differences between gray and white matter may have direct implications on diagnosing, understanding, and eventually manipulating mechanical phenomena during neurodevelopment including lissencephaly, polymicrogyria, brachycephaly, plagiocephaly, and hydrocephalus.

## Acknowledgements

This work was supported by the German National Science Foundation Grant STE 544/50-1 to Silvia Budday and Paul Steinmann, by the Stanford Bio-X Interdisciplinary Initiatives Program, by the National Science Foundation CAREER award CMMI 0952021, and by the National Institutes of Health Grant U01 HL119578 to Ellen Kuhl.

## REFERENCES

- Bayly, P.V., Taber, L.A., Kroenke, C.D., 2014. Mechanical forces in cerebral cortical folding: a review of measurements and models. *J. Mech. Behav. Biomed. Mater.* 29, 568–581.
- Blum, M.M., Ovaert, T.C., 2012. Experimental and numerical tribological studies of a boundary lubricant functionalized poro-viscoelastic PVA hydrogel in normal contact and sliding. *J. Mech. Beh. Biomed. Mater.* 14, 248–258.
- Böl, M., Kruse, R., Ehret, A.E., 2013. On a staggered iFEM approach to account for friction in compression testing of soft materials. *J. Mech. Behav. Biomed. Mater.* 27, 204–213.
- Böl, M., Ehret, A.E., Leichsenring, K., Weigert, C., Kruse, R., 2014. On the anisotropy of skeletal muscle tissue under compression. *Acta Biomater.* 10, 3225–3234.
- Budday, S., Raybaud, C., Kuhl, E., 2014. A mechanical model predicts morphological abnormalities in the developing human brain. *Sci. Rep.* 4, 5644.
- Budday, S., Steinmann, P., Kuhl, E., 2014. The role of mechanics during brain development. *J. Mech. Phys. Solids* 72, 75–92.
- Chatelin, S., Constantinesco, A., Willinger, R., 2010. Fifty years of brain tissue mechanical testing: from in vitro to in vivo investigations. *Biorheology* 47, 255–276.
- Chen, S., Bilston, L.E., 2007. Unconfined compression of white matter. *J. Biomech.* 40, 117–124.
- Christ, A.F., Franze, K., Gautier, H., Moshayedi, P., Fawcett, J., Franklin, R.J.M., Karadottir, R.T., Guck, J., 2010. Mechanical difference between white and gray matter in the rat cerebellum measured by scanning force microscopy. *J. Biomech.* 43, 2986–2992.
- Elkin, B.S., Morrison, B., 2013. Viscoelastic properties of the P17 and adult rat brain from indentation in the coronal plane. *J. Biomech. Eng.* 135, 114507.
- Fallenstein, G.T., Hulce, V.D., Melvin, J.W., 1969. Dynamic mechanical properties of human brain tissue. *J. Biomech.* 2, 217–226.
- Feng, Y., Clayton, E.H., Chang, Y., Okamoto, R.J., Bayly, P.V., 2013. Viscoelastic properties of the ferret brain measured in vivo at multiple frequencies by magnetic resonance elastography. *J. Biomech.* 46, 863–870.
- Fountoulakis, M., Hardmeier, R., Höger, H., Lubec, G., 2001. Postmortem changes in the level of brain proteins. *Exp. Neurol.* 167, 86–94.
- Franceschini, G., Bigoni, D., Regitnig, P., Holzapfel, G.A., 2006. Brain tissue deforms similar to filled elastomers and follows consolidation theory. *J. Mech. Phys. Solids* 54, 2592–2620.
- Franze, K., Janmey, P.A., Guck, J., 2013. Mechanics in neuronal development and repair. *Annu. Rev. Biomed. Eng.* 15, 227–251.
- Galford, J.E., McElhaney, J.H., 1970. A viscoelastic study of scalp, brain, and dura. *J. Biomech.* 3, 211–221.
- Garcia, J.A., Pena, J.M., McHugh, S., Jérusalem, A., 2012. A model of the spatially dependent mechanical properties of the axon during its growth. *Comput. Model. Eng. Sci.* 1, 1–22.
- Garo, A., Hrapko, M., van Dommelen, J.A.W., Peters, G.W.M., 2007. Towards a reliable characterization of the mechanical behavior of brain tissue: the effects of post-mortem time and sample preparation. *Biorheology* 44, 51–58.
- Gefen, A., Margulies, S.S., 2004. Are in vivo and in situ brain tissues mechanically similar? *J. Biomech.* 37, 1339–1352.
- Goriely, A., Geers, M.G.D., Holzapfel, G.A., Jayamohan, J., Jerusalem, A., Sivaloganathan, S., Squier, W., van Dommelen, J.A.W., Waters, S., Kuhl, E., 2015. Mechanics of the brain: perspectives, challenges, and opportunities. *Biomech. Model. Mechanobiol.* <http://dx.doi.org/10.1007/s10237-015-0662-4>.
- Green, M.A., Bilston, L.E., Sinkurs, R., 2008. In vivo brain viscoelastic properties measured by magnetic resonance elastography. *NMR Biomed.* 21, 755–764.
- Gupta, S., Carrillo, F., Li, C., Pruitt, L., Puttlitz, C., 2007. Adhesive forces significantly affect elastic modulus determination of soft polymeric materials in nanoindentation. *Mater. Lett.* 61, 448–451.
- Hamhaber, U., Sack, I., Papazoglou, S., Rump, J., Klatt, D., Braun, J., 2007. Three-dimensional analysis of shear wave propagation observed by in vivo magnetic resonance elastography of the brain. *Acta Biomater.* 3, 127–137.
- Holland, M.A., Miller, K.E., Kuhl, E., 2015. Emerging brain morphologies from axonal elongation. *Ann. Biomed. Eng.* <http://dx.doi.org/10.1007/s10439-015-1312-9>, in press.
- Holzapfel, G.A., Ogden, R.W., 2013. Elasticity of biopolymer filaments. *Acta Biomater.* 9, 7320–7325.
- Hutchinson, B.L., Hutchinson, L.A.D., Thompson, J.M.D., Mitchell, E.A., 2004. Plagiocephaly and brachycephaly in the first two years of life: a prospective cohort study. *Pediatrics* 114, 970–980.
- Jérusalem, A., Dao, M., 2012. Continuum modeling of a neuronal cell under blast loading. *Acta Biomater.* 8, 3360–3371.
- Kaster, T., Sack, I., Samani, A., 2011. Measurement of the hyperelastic properties of ex vivo brain tissue slices. *J. Biomech.* 44, 1158–1163.
- Kohn, J.C., Ebenstein, D.M., 2013. Eliminating adhesion errors in nanoindentation of compliant polymers and hydrogels. *J. Mech. Behav. Biomed. Mater.* 20, 316–326.
- Kruse, S.A., Rose, G.H., Glaser, K.J., Manduca, A., Felmlee, J.P., Jack, C.R., Ehman, R.L., 2008. Magnetic resonance elastography of the brain. *NeuroImage* 39, 231–237.
- Lang, G.E., Stewart, P.S., Vella, D., Waters, S.L., Goriely, A., 2014. Is the Donnan effect sufficient to explain swelling in brain tissue slices? *J. R. Soc. Interface* 11, 20140123.
- Liu, K., VanLandingham, M.R., Ovaert, T.C., 2009. Mechanical characterization of soft viscoelastic gels via indentation and optimization-based inverse finite element analysis. *J. Mech. Behav. Biomed. Mater.* 2, 355–363.
- Metz, H., McElhancy, J., Ommaya, A.K., 1970. A comparison of the elasticity of live, dead, and fixed brain tissue. *J. Biomech.* 3, 453–458.
- Miller, K., Chinzei, K., 1997. Constitutive modelling of brain tissue: experiment and theory. *J. Biomech.* 30, 1115–1121.
- Miller, K., 2011. *Biomechanics of the Brain*. Springer, New York.

- Moore, D.F., Jérusalem, A., Nyein, M., Noels, L., Jaffee, M.S., Radovitzky, R.A., 2009. Computational biology – modeling of primary blast effects on the central nervous system. *Neuroimage* 47, T10–T20.
- Oliver, W.C., Pharr, G.M., 2004. Measurement of hardness and elastic modulus by instrumented indentation: advances in understanding and refinements to methodology. *J. Mater. Res.* 19, 3–20.
- Pervin, F., Chen, W.W., 2009. Dynamic mechanical response of bovine gray matter and white matter brain tissues under compression. *J. Biomech.* 42, 731–735.
- Prange, M.T., Margulies, S.S., 2002. Regional, directional, and age-dependent properties of the brain undergoing large deformation. *J. Biomech. Eng.* 124, 244–252.
- Prevost, T.P., Balakrishnan, A., Suresh, S., Socrate, S., 2011. Biomechanics of brain tissue. *Acta Biomater.* 7, 83–95.
- Raybaud, C., Widjaja, E., 2011. Development and dysgenesis of the cerebral cortex: malformations of cortical development. *Neuroimag. Clin. N. Am.* 21, 483–543.
- Richman, D.P., Stewart, R.M., Hutchinson, J.W., Caviness, V.S., 1975. Mechanical model of brain convolitional development. *Science* 189, 18–21.
- Sun, T., Hevner, R.F., 2014. Growth and folding of the mammalian cerebral cortex: from molecules to malformations. *Nat. Neurosci.* 15, 217–231.
- Tamura, A., Hayashi, S., Watanabe, I., Nagayama, K., Matsumoto, T., 2007. Mechanical characterization of brain tissue in high-rate compression. *J. Biomech. Sci. Eng.* 2, 115–126.
- van Dommelen, J.A.W., van der Sande, T.P.J., Hrapko, M., Peters, G.W.M., 2010. Mechanical properties of brain tissue by indentation: interregional variation. *J. Mech. Behav. Biomed. Mater.* 3, 158–166.
- Xu, G., Knutsen, A.K., Dikranian, K., Kroenke, C.D., Bayly, P.V., Taber, L.A., 2010. Axons pull on the brain, but tension does not drive cortical folding. *J. Biomech. Eng.* 132, 071013.
- Zhang, J., Michalenko, M.M., Kuhl, E., Ovaert, T.C., 2010. Characterization of indentation response and stiffness reduction of bone using a continuum damage model. *J. Mech. Behav. Biomed. Mater.* 3, 189–202.
- Zilles, K., Palomero-Gallagher, N., Amunts, K., 2013. Deveopment of cortical folding during evolution and ontogeny. *Trends Neurosci.* 36, 275–284.